

Thermoelectric power of Cerium and Ytterbium intermetallics

V. Zlatić¹, I. Milat^{1,2}, B. Coqblin³ and G. Czycholl⁴

¹Institute of Physics, Bijenička cesta 46, P. O. Box 304, HR-10001 Zagreb, Croatia

²Institute for Theoretical Physics, ETH-Hönggerberg, CH-8093 Zürich, Switzerland

³Universite Paris-Sud, Bt. 510, Centre d'Orsay, 91405 - Orsay - Cedex, France

⁴Institute for Theoretical Physics, Bremen University, D-28334 Bremen, Germany
(November 5, 2018)

Temperature dependence of the thermoelectric power (TEP) of metallic systems with cerium and ytterbium ions exhibits some characteristic features, which can be used to classify these systems into distinct categories. We explain the observed properties in terms of the Kondo effect modified by the crystal field (CF) splitting and relate various shapes to different energy scales that characterize scattering of conduction electrons on Ce and Yb ions at different temperatures. The low- and high-temperature behaviors are calculated for different fixed point models and the overall shape of the TEP is obtained by interpolation. At high temperatures we use the Coqblin-Schrieffer model (CSM) and calculate the thermoelectric power by the perturbation expansion with renormalized coupling constants. Performing the renormalization by the 'poor man's scaling' (PMS), we find for large CF splitting two Kondo scales, T_K and $T_K^H \gg T_K$. The thermopower obtained in such a way exhibits a large maximum at about T_K^H , and a sign change at about T_K . The PMS also shows that for $T \ll T_K^H$ the f level behaves as an effective multiplet with the degeneracy of the CF ground state and Kondo scale T_K . Thus, we assume that the low-temperature fixed point models do not require the CF splitting. The properties of dilute Ce and Yb alloys are obtained for $T \leq T_K$ from an effective spin-degenerate single-impurity Anderson model (SIAM). The parameters of SIAM are such that its effective Kondo scale coincides with the Kondo scale T_K of the CSM. The stoichiometric compounds are described by an effective spin-degenerate periodic Anderson model (PAM), such that its characteristic energy scale T_0 is the same as T_K . The transport coefficients of PAM and SIAM are calculated by perturbation theory. The interpolation between the Anderson model results, valid for $T \leq T_K$, and the CSM, results valid for $T \geq T_K$, provides a qualitative explanation of the TEP of most Ce and Yb intermetallics.

71.27.+a, 71.28.+d, 72.15.QM, 72.15.Jf

Introduction

The thermo-electric properties of intermetallic compounds with Ce and Yb ions with one f electron or f hole show many interesting features and their thermoelectric power (TEP) considered as a function of temperature, $S(T)$, assumes a variety of shapes.^{1–33} The function $S(T)$ is often non-monotonous and in some systems it exhibits a sign change at lowest temperatures. Above 100 K, the TEP can assume giant values, and much of the recent interest in heavy fermion thermo-electricity is due to the belief that some of the new systems, with the thermopower larger than $150 \mu\text{V/K}$, might be useful for application.³⁴ The functional form of $S(T)$ appears to be quite complicated, but systems with similar thermopower exhibit similarities in other thermodynamic and transport properties as well. The shape of $S(T)$ can be used to classify Ce and Yb intermetallics and alloys into distinct groups.²⁸

The thermo-electric anomalies due to the rare earth ions have stimulated a lot of theoretical work.^{35–46} It is now clear that most of the experimental results can be understood in terms of the exchange scattering of conduction electrons on the $4f^1$ state of Ce or the $4f^{13}$ state of Yb provided one takes into account the splitting of the f states due to the crystalline electric field (CF). The com-

plete description would have to consider the many-body effects due to the local correlation and the hybridization of f electrons with the conduction states, together with the point group symmetry of the crystal and the spin-orbit and the CF splittings. Although the solution of such a general model is not available, one can assume, using the usual renormalization group arguments, that the low- and high-temperature behaviors belong to different fixed points. Provided we know the solution of various models pertaining to different fixed points we can then construct the overall temperature dependence of $S(T)$ by interpolation. Here we show that the typical shapes of the thermopower found in metallic systems with Ce and Yb ions can be explained in such a simple way. The magnetic response of these systems has been explained recently using the same approach.

At high temperatures we use the Coqblin-Schrieffer model (CSM), which takes into account the degeneracy and the CF splitting of Ce $4f^1$ electron and Yb $4f^{13}$ hole. Thus, we describe the f ions as local magnetic moments and assume that the scattering of conduction electrons on such moments is incoherent regardless of their concentration. This is consistent with the observation that the high-temperature thermopowers of dilute alloys and stoichiometric compounds are often surprisingly similar.¹⁰ The giant values of $S(T)$ around the

high-temperature maximum are explained very well by the 3rd-order perturbation theory for the transport relaxation time.^{36,41,48,49} The perturbation theory for the CSM can be further improved by renormalizing the coupling constants by the poor man's scaling.^{50,51} The scaling solution⁵²⁻⁵⁴ shows that a large CF splitting Δ leads to two Kondo temperatures, T_K and $T_K^H \gg T_K$. The high-temperature maximum of $S(T)$ relates to T_K^H and the reduction of temperature can lead to a sign change at T_K . Typical values of T_K , T_K^H , and Δ in Ce and Yb system are 10 K, 100 K, and 100 - 1000 K, respectively. However, the renormalized perturbation expansion becomes unreliable around T_K and cannot be used to describe the non-monotonic thermopower found in many heavy fermions below T_K .

To obtain the fixed point models appropriate for the description of the system at low-temperatures, we use the scaling result that the CF split f state of the CSM can be approximated for $T \ll T_K^H$ by an effective multiplet with the degeneracy of the CF ground state. Thus, as regards the low-energy dynamics, we assume that the sole effect of the excited CF states is to provide the right Kondo scale for an effective model. Once the lowest energy scale is set to T_K , the excited f states can be removed from the low-temperature problem. In addition, we assume that for $T \simeq T_K$ the scattering of conduction electrons is incoherent, regardless of the concentration of the rare earth ions. The properties of the system for $T \leq T_K$ are then found by considering the $4f$ ions as an assembly of f levels with the degeneracy of the CF ground state and no CF splitting. The transport and the thermodynamic anomalies are related to the scattering of conduction electrons on such effective f states. However, to allow for the possibility that for large concentration of Ce and Yb ions the ground state of the system could become coherent, we treat the dilute alloys and the stoichiometric compounds in a different way.

In dilute alloys, where the scattering of conduction electrons on rare earth ions remains incoherent down to lowest temperatures, the effective low-temperature problem for the Ce and Yb impurities is described by the single-impurity Anderson model (SIAM). The effective level of the SIAM is assumed to have the same degeneracy as the CF ground state of the $4f^1$ level and the effective parameters are adjusted in such a way that the width of the f -electron Kondo resonance⁵⁴ coincides with the Kondo temperature T_K of the CSM. Thus, we assume that for $T \leq T_K$ the CSM can be represented by the SIAM. The TEP of the SIAM is then found by some accurate method.^{43,44}

In stoichiometric compounds, the problem is somewhat more difficult, because the reduction of temperature leads to the crossover to the coherent regime. We assume that for $T \leq T_K$ the properties of the lattice of Ce or Yb ions are described by a periodic Anderson model (PAM), such that the effective f levels have the same degeneracy as the lowest CF state of the $4f^1$ or $4f^{13}$ electrons. The absence of the excited CF states simplifies the calculations and

the low-temperature transport coefficients of the PAM can be obtained by the self-consistent perturbation theory with respect to the correlation U .⁵⁵ This leads to a characteristic energy scale T_0 , such that for $T \leq T_0$ the model describes a coherent Fermi-liquid state, and for $T \geq T_0$ an incoherent state. That is, above T_0 , we consider the rare earth ions as independent scattering centers for conduction electrons. The effective parameters are now adjusted to give $T_0 \simeq T_K$, and we assume that for $T \leq T_K$ the PAM and the CSM are dynamically equivalent. Above T_K , the physical state begins to deviate from the incoherent high-temperature state of the PAM which neglects the excited CF states. For $T \gg T_K$ the low-energy properties of stoichiometric compounds are described by the CSM with the CF splitting. Once we obtain the solution of various fixed point model, the overall temperature dependence is found by interpolation.

The paper is organized as follows. First we describe the experimental results. Then we present the scaling solution of the CSM and discuss the TEP obtained by the renormalized perturbation theory. Next, we summarize the low-temperature results obtained for the SIAM and the PAM. Finally, we obtain the full TEP by interpolating between various fixed point solutions and use these results to discuss the data.

Classification of the experimental data

The experimental results for TEP of the Ce- and Yb-based intermetallic compounds exhibits some characteristic features, which can be used to divide these systems into several distinct groups.²⁸

The type (a) thermopower is characterized by a deep negative minimum at low temperatures and a broad positive high-temperature peak between 100 K and 200 K. The type (a) behavior is found in a large majority of Ce-based heavy fermion compounds like CeCu_2Si_2 ,^{4,6,9} CePb_3 ,¹⁷ CeCu_2Ge_2 ,^{17,25,28} CePd_2Si_2 ,^{8,28} CePdSn ,³⁰ CePdGe ,³¹ CeAl_3 ,^{6,10} $\text{CeRh}_{2-z}\text{Ni}_z\text{Si}_2$ for small z ,¹⁹ and CePtGe_2 .³¹ It is also found in Yb-based systems like YbAgCu_4 or YbPd_2Si_2 .²¹

The type (b) thermopower is similar to the type (a), except that at very low temperatures the thermopower changes sign again and exhibits an additional positive peak. These features are often found in dilute Ce-alloys, like $\text{Ce}_x\text{La}_{1-x}\text{Ni}$,¹³ $\text{Ce}_x\text{La}_{1-x}\text{Al}_3$,²⁴ $\text{Ce}_x\text{La}_{1-x}\text{Pd}_2\text{Si}_2$,²⁶ and in some concentrated systems like $\text{Ce}_x\text{La}_{1-x}^2$ and $\text{Ce}_x\text{La}_{1-x}\text{Cu}_2\text{Si}_2$,⁵ or stoichiometric compounds CeAl_3 ,^{6,10} or YbAgCu_4 .²¹ The additional low-temperature peak emerges in CePd_2Si_2 with pressure,²⁸ and in $\text{Ce}_x\text{La}_{1-x}\text{Pd}_2\text{Si}_2$ with chemical pressure.²⁶ In some cases the positive low-temperature peak is concealed by the superconducting or magnetic transitions. For example, in CeCu_2Si_2 ⁶ the positive low-temperature upturn does not appear in the zero-field data and it is only seen in an external magnetic field

which suppresses the superconducting transition.

In type (c) systems the low-temperature maximum is more pronounced than in type (b) but the separation to the high-temperature maximum is small and such that the minimum in-between does not extend down to negative values. The sign of $S(T)$ remains in type (c) systems the same at all temperatures. These features are found in dilute systems like $\text{Ce}_x(\text{La}_{1-x}\text{Y}_z)_{1-x}\text{Al}_2$,¹ $\text{Ce}_x\text{La}_{1-x}\text{Cu}_6$,¹² and $\text{Ce}_x\text{La}_{1-x}\text{Ru}_2\text{Si}_2$,¹⁴ in Ce-rich compounds like $\text{Ce}(\text{Pb}_{1-z}\text{Sn}_z)$,¹⁸ CeRu_2Si_2 ,¹⁵ $\text{Ce}(\text{Cu}_z\text{Au}_{1-z})_6$ for small z ,²⁰ and also in $\text{Ce}_x\text{La}_{1-x}\text{Ni}_{0.8}\text{Pt}_{0.2}$,²⁷ $\text{Ce}_x\text{La}_{1-x}\text{Cu}_2\text{Si}_2$,^{29,32} $\text{Ce}_x\text{Y}_{1-x}\text{Cu}_2\text{Si}_2$.³³

The type (d) thermopower exhibits a large high-temperature peak, and perhaps a shoulder on the low-temperature side of that peak. This behavior is found at ambient pressure in CeCu_6 and $\text{Ce}_x\text{La}_{1-x}\text{Cu}_6$,¹² CeInCu_2 ,²² CeCu_3Ga_2 , and CeCu_3Al_2 ,²³ CePnGe ,³¹ and under high pressure in CeCu_2Si_2 ,⁹ CeCu_2Ge_2 ,²⁸ and CePd_2Si_2 .²⁸

Finally, the TEP of shape (e) is found in *valence fluctuators*, where one observes a monotonic increase all the way up to room temperatures. This is seen in CeBe_{13} ,⁹ CePd_3 ,¹¹ CeNi_2Si_2 ,^{19,3} or in CeNi and CeNi_2 .⁷

The border between various categories is not very sharp and the TEP can be transformed from one type to another by changing the environment of 4f ions. In addition to the already listed examples, we mention $\text{Ce}_x\text{La}_{1-x}\text{Cu}_6$,¹² where for $x < 0.5$ one finds two peaks separated by a well resolved minimum, while for $x > 0.9$ only a single hump with a shoulder on the low-temperature side²⁷ remains. Similarly, by changing the concentration of Ce ions, one transforms $S(T)$ of $\text{Ce}_x\text{La}_{1-x}\text{Pd}_2\text{Si}_2$ ²⁶ from type (a) to type (b), that of $\text{Ce}_x\text{La}_{1-x}\text{Cu}_2\text{Si}_2$ ^{5,29,29,32} from type (a) to type (c), and that of $\text{Ce}_x\text{Y}_{1-x}\text{Cu}_2\text{Si}_2$ ³³ from type (a) to type (d). Direct application of pressure (rather than chemical pressure) transforms the TEP of CePd_2Si_2 ,²⁸ CeCu_2Si_2 ⁹ or CeAl_3 ,¹⁶ from type (a) or (b) to type (c) or (d).

Typical behaviors of the TEP are found in the $\text{Ce}_{1-x}\text{La}_x\text{Cu}_2\text{Si}_2$ family of intermetallic compounds for $0.01 \ll x \ll 1.0$ at % of Ce,²⁹ where the TEP data exhibit nearly all the shapes discussed above. (The positive low-temperature peak which is seen in the dilute limit is also found for large concentration of Ce ions, provided one suppresses the superconducting transition by the magnetic field.) The peaks in the thermoelectric power correlate with the logarithmic behavior in the electrical resistance; the magnetic susceptibility data⁴⁷ indicate that above 100 K the local moment is 6-fold degenerate, while below 20 K it appears to be only 2-fold degenerate.

In summary, the experimental data show that the characteristic shapes (a) – (e) appear regardless of the concentration of magnetic ions. The high-temperature thermopower is insensitive to small changes in the concentration of rare earth ions and the thermoelectric anomalies are accompanied by the anomalies in other transport and

thermodynamic properties. We take this behavior as an indication that the TEP anomalies are due to the scattering of conduction electrons from the 4-f state of Ce or Yb ions, and that the high-temperature scattering is incoherent regardless of the concentration of magnetic ions.

High-temperature approximations

The high-temperature properties of the rare earth ions in metallic environment are modeled Coqblin-Schrieffer Hamiltonian⁴⁸ with the CF splitting,

$$H = \sum_{\nu} E_{\nu} a_{\nu}^{\dagger} a_{\nu} + \sum_k \sum_{\nu} \epsilon_k c_{k\nu}^{\dagger} c_{k\nu} - J_0 \sum_{kk'} \sum_{\nu\nu'} c_{k'\nu'}^{\dagger} c_{k\nu} (a_{\nu}^{\dagger} a_{\nu'} - \delta_{\nu\nu'} \langle n_{\nu} \rangle) + \sum_{k,k'} \sum_{\nu} (V_0 - J_0 \langle n_{\nu} \rangle) c_{k'\nu}^{\dagger} c_{k\nu} \quad (1)$$

where all the symbols have their usual meaning. The first term describes the CF-split $4f^1$ state of Ce ions or $4f^{13}$ state of Yb ions, the second term describes the conduction band of width $2D_0$ and a constant density of states ρ_0 , the third term defines the pure (non-diagonal) exchange scattering between $4f^1$ states and band electrons, and the last term is the total (diagonal) potential scattering. We consider here the antiferromagnetic coupling only. The summation over ν is over all the CF states, and J_0 and V_0 are the initial coupling constants, which are assumed to be ν -independent. For simplicity, we represent the $4f^1$ electrons of Ce (the $4f^{13}$ hole of Yb) by their lowest $J = 5/2$ ($J = 7/2$) spin-orbit state, and consider the CF scheme in which the ground state level at E_m and the excited state at E_M are α_m -fold and α_M -fold degenerate, respectively. The energy separation is $E_M - E_m = \Delta$. The model neglects the coherent scattering on Ce ions and is most appropriate for dilute alloys. However, it also applies to concentrated systems at temperatures such that the scattering of conduction electrons on the rare earth ions is incoherent.

Perturbation theory for the thermoelectric power

We describe the high-temperature heat and charge transport by the Boltzmann equation and evaluate the scattering rate for the transport relaxation time up to the 3rd order in J_0 .^{49,36,41} All the computational details can be found in the papers by Cornut and Coqblin⁴⁹ and Bhattacharjee and Coqblin,³⁶ which we refer to as CC and BC, respectively. Here we just quote the thermopower result obtained by BC for the doublet-quartet CF scheme ($\alpha_m = 2$, $\alpha_M = 4$),

$$S = \frac{k_B}{e} \rho_0 \frac{S_{\Delta}}{R_{\Delta}} G_1(\Delta, 0), \quad (2)$$

where S_Δ and R_Δ are given by

$$S_\Delta = 16|J_{Mm}|^2 \left[(2\langle n_m \rangle J_m + 4\langle n_M \rangle J_M) \tanh\left(\frac{\Delta}{2T}\right) - (\tilde{V}_m + J_m \langle n_m \rangle + \tilde{V}_M + J_M \langle n_M \rangle) (\langle n_m \rangle - \langle n_M \rangle) \right], \quad (3)$$

$$R_\Delta = 2 \left[\tilde{V}_m^2 + 2J_m^2 \langle n_m \rangle \left(1 - \frac{\langle n_m \rangle}{2}\right) \right] + 4 \left[\tilde{V}_M^2 + 4J_M^2 \langle n_M \rangle \left(1 - \frac{\langle n_M \rangle}{4}\right) \right] + 16|J_{Mm}|^2 \left(\frac{\langle n_m \rangle}{1 + e^{\Delta/T}} + \frac{\langle n_M \rangle}{1 + e^{-\Delta/T}} \right), \quad (4)$$

and

$$G_1(\Delta, 0) = \frac{\Delta}{T} \left[1 + \frac{\Delta}{2\pi T} \text{Im} \psi' \left(i \frac{\Delta}{2\pi T} \right) \right]. \quad (5)$$

The derivative of the psi-(digamma-) function⁵⁶ is denoted by $\psi'(x)$, the occupancy of the CF states is

$$\langle n_m \rangle = \frac{1}{2 + 4e^{-\Delta/T}}, \quad \langle n_M \rangle = \frac{e^{-\Delta/T}}{2 + 4e^{-\Delta/T}}, \quad (6)$$

and the effective potential scattering is

$$\tilde{V}_m = V_m - J_m \langle n_m \rangle, \quad \tilde{V}_M = V_M - J_M \langle n_M \rangle. \quad (7)$$

Note, $\rho_0 S_\Delta / R_\Delta$ is a dimensionless quantity, ρ_0 is the density of conduction states around the chemical potential μ , and the prefactor in Eq. (2) is $k_B/e \approx 86 \mu\text{V}/\text{K}$.

The qualitative features of the thermopower described by Eq. (2) with constant and isotropic coupling constants ($J_m = J_M = J_{mM} \equiv J_0$, and $\tilde{V}_m = \tilde{V}_M \equiv \tilde{V}$) follow straightforwardly from the asymptotic expansion of the elementary functions in Eq. (2) and can be summarized as follows (detailed analysis can be found in Ref. BC). At temperatures such that $T > \Delta$ the thermopower is small and behaves as $1/T$. The sign of S and its slope depend on the relative size of J_0 and \tilde{V} . As temperature decreases, the thermopower increases up to a large (positive or negative) value at about $T_{max} \simeq \Delta/3$. At temperatures such that $T \ll \Delta$ we find $G_1 \propto T/\Delta$ and $S(T) \propto T$.

For parameters in the physical range one easily finds the peak value of thermopower above $50 \mu\text{V}/\text{K}$ and Eq. (2) captures the essential high-temperature features of Ce and Yb intermetallics.³⁶ At low temperatures, however, perturbative approach leading to Eq. (2) fails and the observed, non-monotonic low-temperature behavior is not reproduced.

Poor man's scaling

The change of sign of the TEP below T_{max} , which is often seen in the experimental data, cannot be obtained from Eq. (2) for any value of J_0 and V_0 . However,

these features follow from the perturbation expansion, provided we renormalize the coupling constants by the poor man's scaling.

The scaling approach to the single-impurity models is explained in great detail in many papers^{50–54} and here we just use these results to calculate the thermopower. The scaling equations are generated by reducing the conduction electron cutoff from D_0 to D and simultaneously rescaling the coupling constant, $J(D)$, so as to keep the low-energy excitations of the total system unchanged.⁵⁰ The solution for the CSM, valid up to the 2nd order in renormalized couplings, reads⁵²

$$\exp\left(-\frac{1}{\rho_0 J}\right) = \left(\frac{T_K}{D}\right)^m \left(\frac{T_K + \Delta}{D + \Delta}\right)^M, \quad (8)$$

where T_K is the Kondo temperature, defined by J_0 and D_0 . For a given set of initial parameters the renormalized coupling constant $J(D)$ is completely characterized by T_K . The result obtained for $m = 2$, $M = 4$, and $\Delta = 330 \text{ K}$ is shown in Fig. 1 as a function of D/T_K^H , where T_K^H is defined below (see Eq. 10). For a given value of D_0 and Δ , the Kondo temperature grows exponentially with J_0 ; for a given D_0 and J_0 the Kondo temperature grows with the CF splitting as $(\Delta/D_0)^M$. The scaling trajectory defined by Eq.(8) diverges at $D = T_K$, such that $J(T)$ can be used to renormalize the weak-coupling theories for $D \gg T_K$ only. Note that the CF splitting lowers the degeneracy of the f level and reduces the Kondo scale from T_K^H to T_K , which extends the validity of the weak-coupling theory to much lower temperatures.

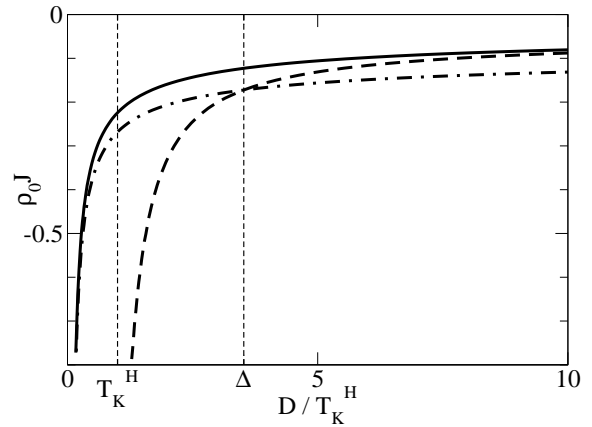


FIG. 1. D dependence of the scaled exchange coupling $J(D)$ of CS Hamiltonian in the case of a ground state doublet and an excited quartet, separated by the CF splitting Δ . Solid curve is the 2nd-order Hanzawa scaled result. Dashed and dot-dashed curves are the high-energy and low-energy asymptotic scaling trajectories appropriate to a sixfold degenerate and a doubly degenerate level, respectively.

The scaling trajectory $J(T)$, defined by Eq. 8) and shown in Fig. 1, has two asymptotic regimes.⁵³ The high-temperature asymptote, $J_H(T)$, is obtained from Eq. (8) by neglecting Δ with respect to D , which leads to

$$\exp\left(-\frac{1}{\rho_0 J_H}\right) = \left(\frac{T_K^H}{D}\right)^N, \quad (9)$$

where T_K^H is the high-temperature Kondo scale given by

$$(T_K^H)^N = (T_K)^m (T_K + \Delta)^M, \quad (10)$$

and $N = m + M$. The same trajectory would be obtained for an effective sextet without the CF splitting, assuming the initial condition $J_H(D_0) = J_0$.

The low-temperature asymptote $J_L(D)$ is obtained by neglecting in Eq. (8) T_K and D with respect to Δ , i.e., by neglecting the effects of the excited CF levels. This identifies $J_L(D)$ as the scaling trajectory of an effective doublet with Kondo scale T_K and the effective coupling

$$\exp\left(-\frac{1}{\rho_0 J_L}\right) = \left(\frac{T_K}{D}\right)^m. \quad (11)$$

Note that the value of T_K in the above expression is defined by Eq. (8) with the initial condition $J(D_0) = J_0$. The initial condition $J_L(D_0) = J_0$ and Eq. (11) would lead to a Kondo temperature T_K^L that would be much lower than T_K , i.e., the Kondo scale that enters Eq.(11) is exponentially enhanced with respect to T_K^L because of CF splitting.

Thus, the scaling analysis shows that the f level behaves at high temperatures as an effective sextet with the scaling trajectory $J_H(D)$ and Kondo scale T_K^H , while at low temperatures it behaves as an effective doublet with the scaling trajectory $J_L(D)$ and Kondo scale $T_L = T_K$. The scaling trajectory $J(D)$ of the CSM with the CF splitting interpolates between these two asymptotic regimes. Here, we discussed the scaling solution obtained by the 2nd-order perturbation expansion but the same behavior is obtained in the next leading order.⁵³

Renormalized perturbation expansion

The scaling theory can be used to obtain a simple description of the overall magnetic and transport properties of the CSM. It provides the thermopower in the following way. We reduce the conduction-electron half-bandwidth from D_0 to $D = A k_B T$, where A is a numerical constant of the order of unity, and find the effective couplings $J(T)$, $V_m(T)$, and $V_M(T)$. Next, we notice that the reduction of the bandwidth does not change the form of the Hamiltonian, and that the form of the response functions obtained by perturbation expansion in terms of the effective coupling constants remain invariant with respect to the scaling. Thus, to obtain the poor man's scaling result for the thermopower we introduce the temperature-dependent cutoff $D = A k_B T$, find $J(T)$ from Eq.(8), and substitute this renormalized expansion parameter in the expressions (2) - (7).

To apply the scaling result to a specific Ce or Yb system we have to determine the degeneracy and the splitting of the CF levels, estimate the initial coupling constant (or T_K), and choose the cutoff constant A . The

thermopower obtained by the renormalized perturbation theory depends on the magnitudes of the Kondo temperature, the potential scattering, the CF splitting, and the density of states of the conduction electrons at the Fermi level. These parameters are restricted to a rather narrow range by the requirements that the model explain not just the thermopower data but that it also leads to a consistent description of other thermodynamic and transport data of a particular system. We estimate the CF splitting and the degeneracies of the CF states by analyzing the neutron scattering and the high-temperature magnetic anisotropy data. The Kondo temperature T_K , i.e., the initial coupling J_0 , can be obtained from the magnetic susceptibility data, provided we know how to extract the single-ion contribution from the experimental results⁴⁷. The high-temperature Kondo scale T_K^H is then found from Eq. (10). The relationship between T_K and $J(T)$ depends to some extent on the scaling procedure and the value of the cutoff constant A . Our analysis of the thermopower of the CSM is based on the 2nd-order scaling equation⁵² and we use, for simplicity, $A = 1$. The 3rd-order scaling equation⁵³ and/or some larger values of A do not change the TEP in any qualitative way. The potential scattering shows up in the electrical resistance and typical results for the high-temperature phase⁵⁷ indicate rather large values for \tilde{V} .

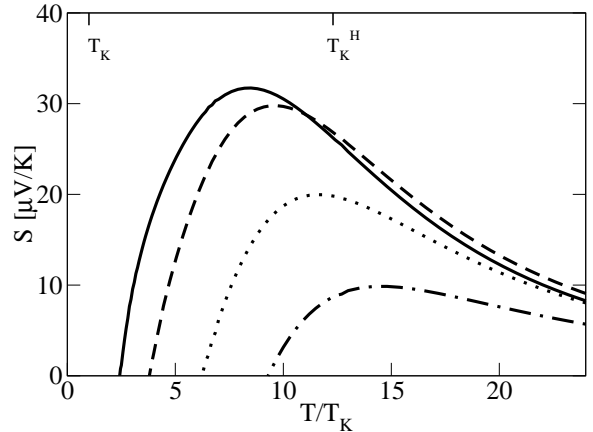


FIG. 2. The thermopower is plotted as a function of reduced temperature T/T_K and for various values of the potential scattering. Dot-dashed curve $\rho_0 \tilde{V} = -0.15$, dotted curve $\rho_0 \tilde{V} = -0.20$, dashed curve $\rho_0 \tilde{V} = -0.35$, solid curve $\rho_0 \tilde{V} = -0.5$. Here we used $T_K = 8$ K and $\Delta = 350$ K, such that $T_K^H = 99$ K.

The thermoelectric power obtained for the doublet-quartet CF scheme, with $\Delta = 350$ K and for several values of T_K and \tilde{V} , is shown in Figs. 2 - 4. The density of conduction states, which enters the thermopower calculations, is set to $\rho_0 = 2.2$ (eV)⁻¹. Fig. 2 shows the effect of \tilde{V} on $S(T)$ for $T_K = 8$ K, $T_K^H = 99$ K, and $\Delta = 350$ K. The details of the shape of $S(T)$ depend in a rather complicated way on the relative magnitude of T_K , \tilde{V} , and Δ . For large \tilde{V} the value of T_{max} is mainly determined by T_K^H , which is related to T_K and Δ by Eq. (10).

For small values of \tilde{V} , the TEP changes sign before the full maximum can develop. The crossing temperature T_x , where $S(T)$ changes sign, i.e. $S(T_x) = 0$, increases as $|\tilde{V}|$ decreases.

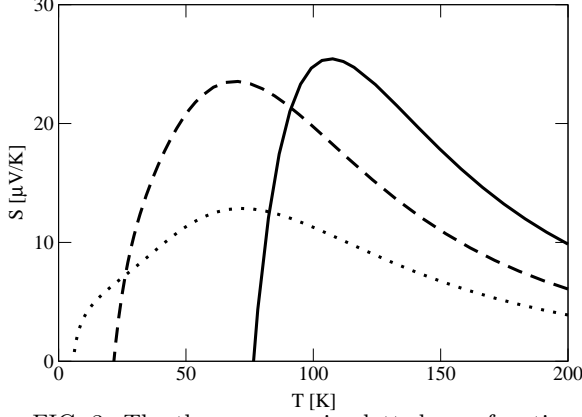


FIG. 3. The thermopower is plotted as a function of temperature for $\rho_0\tilde{V} = -0.35$ and $\Delta = 350$ K, and for three values of T_K . Dotted curve $T_K = 2$ K, $T_K^H = 63$ K, dashed curve $T_K = 8$ K, $T_K^H = 99$ K, solid curve $T_K = 32$ K, $T_K^H = 158$ K.

Fig. 3 shows $S(T)$ for $\Delta = 350$ K, $\tilde{V} = 0.35$, and for 3 values of T_K . For such a large value of $\rho_0\tilde{V}$, we find that the maximum of $S(T)$ is around T_K^H and that T_x scales approximately with T_K . Fig. 4 shows the effect of Δ on $S(T)$ for $T_K = 8$ K and $\tilde{V} = -0.35$. The position of T_{max} is rather well described by T_K^H , while the value of T_x is not much changed by Δ , as it mainly depends on T_K . The overall features of $S(T)$ shown in Figs.3 - 4 follow straightforwardly from expressions (2) - (4). Eq.(3) contains the products of logarithmic functions and at high temperatures, where $J(T)$ changes very slowly, $S(T)$ reduces to the BC expression³⁶. Eq. (3) shows that the sign of the thermopower is determined by the temperature dependent factor $J(T) - \tilde{V}$, and that $S(T)$ approaches zero for $J(T) \simeq \tilde{V}$.

However, to make a quantitative analysis of $S(T)$ close to T_x , we should not neglect the higher-order terms in the expansion of transport integrals. The 3rd-order perturbation theory provides an indication that $S(T)$ changes sign below T_{max} and exhibits non-monotonic features. Since $S(T)$ must vanish at $T = 0$, the finite value of T_x must lead to a low-temperature minimum, which is here obtained from the exchange scattering, without invoking the interaction effects or long-range antiferromagnetic fluctuations.³⁹

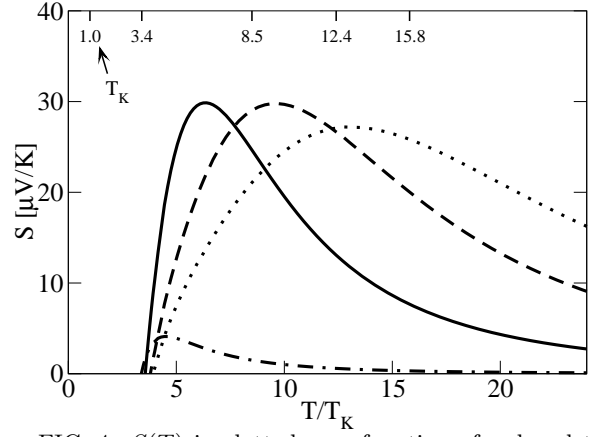


FIG. 4. $S(T)$ is plotted as a function of reduced temperature T/T_K for $\rho_0\tilde{V} = -0.35$ and for various values of the CF splitting. The curves are obtained for $T_K = 8$ K, and the dot-dashed, solid, dashed, and dotted curve correspond to $\Delta = 50$ K ($T_K^H = 27$ K), $\Delta = 200$ K ($T_K^H = 68$ K), $\Delta = 350$ K ($T_K^H = 99$ K), and $\Delta = 500$ K ($T_K^H = 126$ K), respectively.

The properties of the model for $T \leq T_K$ can not be obtained from scaling. On the one hand, Eq. (8) is derived by assuming that thermal fluctuations do not excite too many conduction electrons or holes up to states near the (effective) band edges; this assumption does not hold for $T \leq T_K$, i.e., the scaling breaks down when the effective (renormalized) band edge is of the order T_K . On the other hand, the perturbation theory for the response functions breaks down close to T_K , because the effective coupling constants become too large for the lowest-order perturbation expansion to be valid. However, Fig. 1 indicates that the breakdown of scaling occurs at temperatures such that $J(T) \simeq J_L(T)$, and that the low-energy dynamics of the CSM is rather well described by an effective doublet or quartet. Thus, we neglect the CF splitting at low temperatures and calculate the thermopower of Ce and Yb intermetallics by using the methods that are more accurate than scaling.

Low-temperature approximations

To discuss the low-temperature properties we start from the scaling result that the $4f^1$ or $4f^{13}$ states of the rare earth ions behave for $T \simeq T_K \ll T_K^H$ as effective levels with the degeneracy of the CF ground state. We assume that the coupling of such effective states to the conduction electrons characterizes the Kondo temperature which is the same as T_K of the full CS model, and describe the low-temperature data by models without the CF splitting. Since the reduction of temperature could lead to coherent scattering of conduction electrons on rare earth ions, stoichiometric compounds are treated differently from dilute alloys.

In ordered compounds, we assume that the coherence temperature of the lattice of rare earth ions, T_0 , is not much different from T_K , the lowest Kondo temperature of the CS model. Since the crossover from the full CF multiplet to an effective low-temperature CF state takes place much above T_K , we neglect the CF splitting in the coherent regime. Thus, for $T \leq T_0$ we describe the stoichiometric compounds by the periodic Anderson model (PAM) which has the degeneracy of the lowest CF state and adjust the effective parameters in such a way that the low-energy scale of the PAM coincides with T_K of the CSM. Here we use the twofold degenerate PAM defined by the Hamiltonian

$$H = \sum_{i\sigma} E_f a_{i\sigma}^\dagger a_{i\sigma} + \sum_k \sum_{\sigma} \epsilon_k c_{k\sigma}^\dagger c_{k\sigma} + (V \sum_k \sum_{i\sigma} e^{ikR_i} c_{k\sigma}^\dagger a_{i\sigma} + h.h.) + U \sum_i a_{i\uparrow}^\dagger a_{i\uparrow} a_{i\downarrow}^\dagger a_{i\downarrow}, \quad (12)$$

where σ labels two spin states of the localized level, E_f is the unrenormalized position of the effective CF ground state, V is the hybridization, and U is the Coulomb repulsion. We consider the case where the f level is below the Fermi level, and the width of the f band W is smaller than the on-site correlation.

A simple but non-trivial approximation to study the PAM is provided by the 2nd-order perturbation theory (SOPT) with respect to the correlation U . The SOPT, which may be regarded as the simplest extension of Hartree-Fock theory, properly reproduces Fermi liquid properties and mass enhancement, and it reproduces a characteristic low-temperature scale T_0 . A disadvantage of the SOPT is the fact that this T_0 has not the proper (non-analytic) dependence on the model parameters (hybridization V and correlation U , in particular), as it should according to the Schrieffer-Wolff transformation. But on the other hand, arbitrarily large mass enhancements and any value of T_0 can be achieved in SOPT by choosing appropriate values for the parameters V and U . Therefore one can choose the parameters of the effective PAM in such a way that T_0 corresponds to the true T_K of the CS model. The SOPT is most easy to apply in the limit of high dimensions $d \rightarrow \infty$,⁵⁸ because then the self-energy is \mathbf{k} -independent (site-diagonal), which is already a good additional approximation for the realistic dimension $d = 3$. Consistent with the site diagonality of the self-energy is the vanishing of vertex corrections. Then the transport coefficients can be calculated from the Kubo formula. The static (zero-frequency) conductivity is given by⁵⁵

$$\sigma_{xx} = \frac{e^2 a^{2-d}}{2\pi\hbar} t^2 \int dE \left(-\frac{df}{dE} \right) L(E), \quad (13)$$

where a is the lattice constant, d the dimension, t the hopping matrix element of the band electrons, $f(E)$ the Fermi function, and the function $L(E)$ is given by

$$L(E) = \frac{2}{N} \sum_{\mathbf{k}\sigma} (\text{Im} G_{\mathbf{k}\sigma}^c(E + i0))^2. \quad (14)$$

The function

$$G_{\mathbf{k}\sigma}^c(z) = \frac{1}{z - \frac{V^2}{z - E_f - \Sigma(z)} - \epsilon_k} \quad (15)$$

is the band electron Green's function of the PAM, and $\Sigma(z)$ the it f-electron self-energy, which we determine approximately within SOPT. The TEP is also determined by the function $L(E)$ according to

$$S = \frac{\int dE \left(-\frac{df}{dE} \right) (E - \mu) L(E)}{eT \int dE \left(-\frac{df}{dE} \right) L(E)} \quad (16)$$

As mentioned above, the SOPT yields a characteristic low-temperature scale T_0 which can be determined or defined as follows. The it f-electron density of states (DOS) at the chemical potential μ is strongly temperature-dependent and decreases as temperature increases on the scale T_0 towards an asymptotic T-independent value. Therefore, T_0 can be defined as the half-width of the T-dependent part of the it f-DOS at μ . When calculating the T-dependence of the resistivity $R(T) = 1/\sigma_{xx}$ from (13), one obtains for most choices of the parameters the following characteristic behavior: A residual resistivity approaching zero for $T \rightarrow 0$, a T^2 dependence for very low T as expected for Fermi liquids, a nearly linear increase with increasing T for $T < T_0$, a maximum of $R(T)$ exactly at T_0 , and an $R(T)$ decreasing with increasing T (and thus behaving similarly as in the case of incoherent scattering from magnetic impurities) for $T > T_0$.

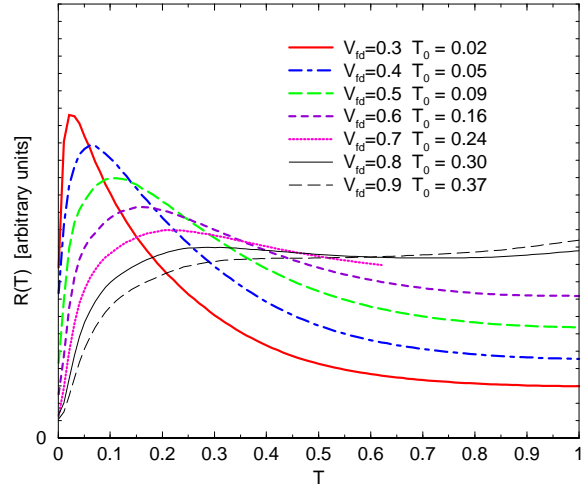


FIG. 5. The resistivity of the periodic Anderson model is shown for various values of the hybridization parameter as a function of temperature measured in units of the band-width W . The total number of electrons per site is $n_{tot} = 2.2$ and the number of f holes is $n_f^{hole} = 0.9$. The value of the Coulomb correlation is $U/W = 1$ and the corresponding low-energy scale T_0 is indicated in the figure.

As an example, we consider the model with more than one f electron per site. This would correspond to Yb systems in which the number of f holes is restricted by large Coulomb correlation to $n_f^{hole} \leq 1$. The numerical results are shown in Fig. 5, where $R(T)$ is plotted versus temperature for the model with the total number of electrons per site $n_{tot} = 2.2$, the occupancy of the f holes $n_f^{hole} = 0.9$, and for different values of hybridization V . For fixed other parameters the hybridization V determines the low-temperature scale T_0 , which is indicated in the figure. The calculations are performed for $U/W = 1$. Remarkably, as long as there is a maximum in $R(T)$, it is very close to T_0 as determined by the f DOS criterion described above. For too large V and T_0 (and the corresponding less strong mass enhancement) there is no longer a true maximum in $R(T)$ but only a plateau behavior.

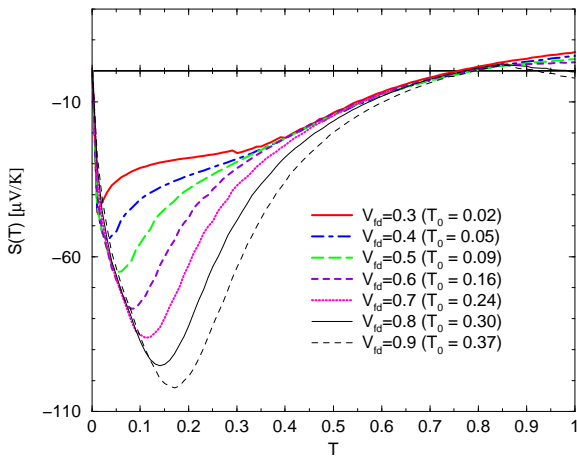


FIG. 6. The thermopower of the periodic Anderson model is shown for various values of the hybridization parameter as a function of temperature, measured in units of the band-width W . The total number of electrons per site is $n_{tot} = 2.2$ and the number of f holes is $n_f^{hole} = 0.9$. The value of the Coulomb correlation is $U/W = 1$ and the corresponding low-energy scale T_0 is indicated in the figure.

Corresponding results for the thermopower are shown in Fig. 6. Note that one obtains $S(T)$ in its natural units (using $k_B/e \approx 86 \mu V/K$) from (16), as the "arbitrary" units (prefactor of (13)) cancels due to the quotient. The initial sign of $S(T)$ depends on the slope of $L(E)$ at the Fermi level and the temperature variation of $S(T)$ reflects the structure of the DOS within the Fermi window. Fig. 6 shows typical results for $S(T)$ of Yb systems, with a large negative low-temperature peak. Obviously $S(T)$ is strongly temperature-dependent and its absolute value is very large, namely of the magnitude 50 - 100 $\mu V/K$. It has an extremum (negative minimum in the plot) at a temperature T_1 , which scales linearly with T_0 , i.e., $T_1 = aT_0$.

For the parameters used for the figure we have $a \approx 0.5$,

but the exact value of a depends on other parameters (U , n_f etc.) as well. This extremum in $S(T)$ also exists in the situation when the resistivity $R(T)$ exhibits no maximum but only a plateau behavior. The absolute value $|S(T_1)|$ at the extremum can even increase with increasing T_0 , i.e., according to this result it is not necessarily the most "heavy" fermion systems that exhibit the largest values of the TEP. In any case, in the low-temperature regime, $T \leq T_0$, this approach yields a TEP of the correct absolute magnitude and qualitative behavior, in particular an extremum, which is characteristic for the TEP experimentally observed in many heavy fermion systems. Of course for intermediate and high T the features due to the CF splitting cannot be reproduced within this SOPT treatment of the PAM, as only the twofold degenerate PAM was used, which has no higher CF-split f levels included.

Single-impurity case

The transport properties of dilute Ce and Yb alloys with the doubly degenerate CF ground state are obtained at temperatures below T_K from the single-impurity spin-1/2 Anderson model. We assume that the number of f electrons (holes) is slightly above (below) one for each Ce (Yb) impurity, and we consider an asymmetric model. The effective parameters of the SIAM are adjusted in such a way that the width of its Kondo resonance coincides with the Kondo temperature T_K of the CSM with CF splitting.

The TEP of a spin-degenerate SIAM, in the absence of the non-resonant scattering channels, has been calculated by various methods and is well understood. We are interested in the low-temperature behavior obtained for $U/\pi\Gamma \gg 1$, where U denotes the f-f correlation and $\Gamma = \pi\rho_F V^2$ is the half-width of the f level due to the hybridization with conduction states. (Here, ρ_F is the density of conduction states at the Fermi level.) The numerical renormalization group calculations (NRG) of Costi, Hewson and Zlatić^{42,43} (in what follows referred to as CHZ) and the perturbation theory⁴⁴ show that $S(T)$ is closely related to the Kondo resonance. In the absence of any potential scattering the behavior of the TEP follows simply the temperature dependence of the f -electron spectral function within the Fermi window. The results for the $4f^1$ electron (and analogous results for the $4f^{13}$ hole) can be summarized as follows.⁴²⁻⁴⁴ Close to $T = 0$ the system is in the Fermi liquid (FL) regime, which is characterized by an asymmetric Kondo resonance of the width T_K , centered above the Fermi energy, E_F . This leads to a typical Fermi liquid power law,

$$S(T) = \frac{\pi^2 k_B}{3|e|} \frac{T}{T_K} \cot \eta_0(E_F), \quad (17)$$

where $\eta_0(E_F)$ is the resonant phase shift due to the scattering of conduction electrons on the f state. It is related

to n_f by the Friedel sum rule, $\eta_0(E_F) = \pi n_f/2$, so that for $n_f < 1$ ($n_f > 1$) the initial slope of the TEP is positive (negative). In heavy fermions, where temperatures of the order of T_K are easily accessible, the TEP grows rapidly with temperature ($\pi^2 k_B/3|e| = 284 \mu\text{V}/K$) and can assume giant values. At elevated temperatures the Fermi liquid behavior breaks down, because the spectral weight is transferred out of the low-energy region and the Kondo resonance disappears. For $T > T_K$, the system enters the local-moment (LM) regime. Here, for $n_f > 1$, the maximum of the spectral function shifts from above to below E_F and the TEP is negative. For $n_f < 1$, we find that in the LM regime the TEP is positive.

These simple features are modified in the presence of non-resonant scattering at the impurity site, because the interference between the resonant and the non-resonant channels leads to vertex corrections, which have drastic effects on the thermopower. These effects have been analyzed in detail in CHZ, and here we use that theory to study the changes in $S(T)$ induced by a small variation in n_f . Such changes in n_f could be induced by pressure or doping (chemical pressure). The TEP is still given by the expression (16), but the evaluation of the Kubo formula gives for $L(\omega)$ the result⁴³

$$\frac{1}{L(\omega)} = \frac{1}{L_0(\omega, T)} \left[\cos 2\eta_1 - \frac{\text{Re } G(\omega)}{\text{Im } G(\omega)} \sin 2\eta_1 \right] + \rho_n. \quad (18)$$

Here, η_1 is the non-resonant phase shift, $\rho_n \simeq \sin^2(\eta_1)$ is the residual resistance due to the non-resonant scattering, and $L_0(\omega)$ is the transport relaxation time due to the resonant scattering,

$$\frac{1}{L_0(\omega)} = -\frac{\Gamma}{\pi} \text{Im } G(\omega), \quad (19)$$

(for details of derivation see CHZ). The resonant Green's function in Eq. (19) has been calculated by the NRG methods⁴³ and the results were used to study the thermopower at the crossover from above to below T_K . However, in the presence of CF splitting we do not need the resonant Green's function of the spin-1/2 problem for temperatures much above T_K . In the Fermi liquid regime it is sufficient to evaluate $G(\omega)$ by an approximate method⁵⁹ that interpolates between the 2nd-order weak-coupling expression (in what follows referred to as MR) and the exact atomic limit. This simple approximation is quite accurate for $T \leq T_K$; it gives the spectral function and the thermoelectric power similar to the NRG results of CHZ even for $U/\pi\Gamma \gg 1$. The approximation becomes unphysical for $T \gg T_K$ but here we are not interested in such high temperatures where the spin-1/2 model becomes inadequate anyway. The approximation is based on the Dyson equation,

$$G(\omega) = \frac{1}{\omega - \epsilon_l + i\Gamma - U n_f - \Sigma(\omega)}, \quad (20)$$

with ϵ_l determined iteratively in such a way that the number of electrons per spin,

$$\tilde{n} = \int d\omega f(\omega) \left(-\frac{1}{\pi} \text{Im } G \right), \quad (21)$$

equals n_f . The self-energy $\Sigma(\omega)$ is defined by the Martin-Rodero interpolation,

$$\Sigma(\omega) = \frac{\tilde{\Sigma}^{(2)}(\omega)}{1 - \frac{(1-n_\sigma)U + \epsilon_l - \epsilon_0}{n_\sigma(1-n_\sigma)U^2} \tilde{\Sigma}^{(2)}(\omega)}, \quad (22)$$

where, ϵ_0 is the energy of the virtual bound state of the $U = 0$ Anderson model with n_f electrons, and $\tilde{\Sigma}^{(2)}(z)$ is the 2nd-order self-energy calculated with the unperturbed propagators of this auxiliary $U = 0$ model (for details see Ref. MR).

The thermopower obtained by this approximation is plotted in Fig. 7 as a function of temperature and for several values of n_f . We consider the case of strong correlation, $U/\pi\Gamma = 8$, and assume a small non-resonant scattering, $\eta_1 = -0.1$ (the effect of ρ_n on $S(T)$ is neglected). The value of T_K (in units of $\pi\Gamma$) is estimated from the f spectral function that we obtain from the Dyson equation (20). We use two different estimates: (i) we associate T_K with the full width at half the maximum (FWHM) of the Kondo resonance at $T = 0$, and (ii) we identify T_K as the half-width of the temperature-dependent part of the f -electron spectral function at the chemical potential. The value of T_K obtained by either method is almost the same, and we find that the reduction of n_f enhances T_K .

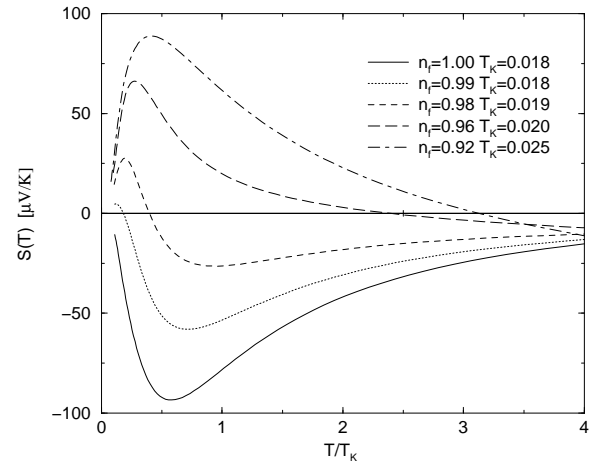


FIG. 7. The thermopower of the single-impurity Anderson model is shown for various f occupation as a function of temperature, measured in units of T_K . The value of the Coulomb correlation is $U/\pi\Gamma = 8$ and the corresponding Kondo scale T_K is indicated in the figure.

The $n_f = 1$ curve corresponds to an extreme Kondo limit, where $S(T)$ goes rapidly to a large negative peak at about $T \simeq T_K/2$, and then decreases gradually but

remains negative within the physically relevant temperature range $T \leq T_K$. The effect of the non-resonant phase shifts is very important, because at half-filling ($n_f = 1$) the model is electron-hole symmetric and in the absence of the non-resonant phase shifts the thermopower vanishes. The $n_f = 0.98$ and $n_f = 0.99$ curves are still Kondo-like, but the reduction of η_0 from $\pi/2$ gives rise to a positive initial slope of $S(T)$, such that $S(T)$ develops a well defined positive maximum before decreasing sharply to negative values for temperatures between $T_K/2$ and T_K . Finally, the $n_f = 0.96$ and $n_f = 0.92$ curves remain positive for $T \leq T_K$. Further reduction of n_f does not bring any new qualitative features, except that the maximum of $S(T)$ becomes higher and shifts to higher temperatures. By changing the other parameters, like the correlation or the non-resonant phase shifts, we find a similar set of curves, that could be classified in the same way as the curves shown in Fig. (7).

The low-temperature thermopower results shown in Fig. (7) exhibit all the features found in dilute Ce alloys for $T \leq T_K$. Reflecting the curves on the $S = 0$ axis, gives $S(T)$ that correspond to the Yb alloys, with one magnetic f hole.

Discussion of different cases (a) to (e) and conclusion

The overall temperature dependence of the TEP of Ce and Yb intermetallics is found by interpolating between the results for the Anderson model, valid below T_K , and the CSM results, valid above T_K . The essential features of $S(T)$ are due to the Kondo effect modified by CF splitting, and various shapes are the consequence of different energy scales that characterize the low- and high-temperature behavior. The details, however, depend not just on the single parameter T_K , but on other parameters of the model as well. Here we discuss, for simplicity, the thermopower due to the cerium ions with a single electron in the $4f^1$ configuration. The results pertaining to ytterbium ions with a single hole in the $4f^{13}$ configuration are obtained by reflecting the $S(T)$ on the temperature axis.

In (a)- and (b)-type systems a large CF splitting of Ce f states generates two distinct energy scales, which are seen as two Kondo temperatures of the CS model, T_K and $T_K^H \gg T_K$. The high-temperature Kondo scale describes a sixfold degenerate CF multiplet with a large thermopower. Typically, T_K^H is between 30 and 100 K and the maximum value of the thermopower can exceed $150 \mu\text{V/K}$. The low-temperature scale, defined by T_K , is of the order of 1 to 10 K. A twofold or fourfold degenerate CF ground state gives rise, below T_K , to an additional structure in $S(T)$. In periodic systems, the onset of coherence reverses the sign of the thermopower below T_K and gives rise to a large negative peak around $T_0/2 \simeq T_K/2$. The behavior of $S(T)$ in the $T = 0$ limit depends on the band filling and the value of the f-d hy-

bridization: for systems close to the electron-hole symmetry $S(T)$ is positive for $n_f < 1$ and negative for $n_f > 1$. Combining these results with the $T \leq T_K$ results one obtains the thermopower of the (a) or (b) type. In dilute Ce alloys the sign of the low-temperature thermopower is determined by the non-resonant phase shifts. Type (b) behavior is obtained here for a ground CF-level that gives rise to a positive thermopower around $T_K/2$ and a negative one above T_K . For sufficiently different values of T_K and T_K^H the $S(T)$ has two well resolved positive peaks separated by a negative minimum. Changing the sign of the non-resonant phase shifts one reverses the sign of the low-temperature thermopower and finds the (a)-type thermopower: there is a deep negative minimum around $T_K/2$, followed by a positive maximum around T_K^H . The type-(a) and type-(b) systems can be classified as Kondo systems with large CF splitting. The crossover from the high- to the low-temperature fixed point is accompanied by the sign change of the TEP.

The type-(c) behavior can arise in two ways. In the first case, the low- and high-temperature maxima overlap, giving a two-hump structure. That is, the CF splitting is not large enough to generate sufficiently different Kondo scales for the negative minimum to occur. In the second case, the CF splitting might be large but the potential scattering is also large enough to prevent the thermopower due to the CF ground state from changing sign for $T \leq T_K$. Thus, the crossover from the low- to high-temperature fixed point occurs at T_K without the change of sign of $S(T)$. The two LM regimes are still well resolved but $S(T)$ is always positive.

The type-(d) thermopower is obtained for Kondo systems with small CF splitting, such that the low- and high-temperature thermopower peaks overlap, and we see but a single peak with, perhaps, a shoulder on the low-temperature side. In the absence of the CF splitting there is just a single thermopower peak at about $T_K/2$. The sixfold degenerate $4f^1$ electron of Ce ions has a large Kondo scale and huge positive thermopower. (The eightfold degenerate $4f^{13}$ multiplet of Yb ions could lead to even larger negative thermopower.)

In valence fluctuators, the f level is close to the chemical potential and Ce ions fluctuate between two configurations. The thermopower of such a system increases monotonically to a large positive (or negative) value. The characteristic energy scale is defined by the width of the f level, and $S(T)$ might reach very large values.

Finally, we remark that in Kondo systems with Ce ions the application of pressure (or positive chemical pressure) enhances T_K and transforms an (a)- or (b)-type thermopower to a (c)- or (d)-type one. The negative (chemical) pressure reduces T_K and gives rise to a reversed behavior. In Kondo systems with Yb ions the pressure and chemical pressure have the opposite effect than in Ce systems. We hope this simple explanation of the overall behavior of the thermopower of Ce and Yb systems to facilitate the search for optimal thermoelectrics.

Acknowledgment. We acknowledge useful comments

from I. Aviani, B. Horvatić, A. Hewson, J. Freericks, M. Očko, C. Geibel J. Sarrao, and F. Steglich. One of us (V.Z.) gratefully acknowledges the financial support from the Swiss NSF (project number 7KRPJ065554-01/1).

-
- ¹ F. Steglich, Festkoerperprobleme XVII, 319 (1977)
² T. S. Petersen et al., J. Appl. Phys. **50**, 6363 (1979),
³ E. M. Levin et al., Sov. Phys. Solid State **23**, 1403 (1981)
⁴ H. Schneider et al., Solid State Commun. **48** 1093 (1983)
⁵ F. G. Aliev et al., Sov. Phys. Solid State **26** 682 (1984)
⁶ G. Sparn et al. J. Magn. Magn. Mater. **47 & 48**, 521 (1985)
⁷ Gottwick et al., Magn. Magn. Mater. **47 & 48**, 536 (1985)
⁸ A. Amato and J. Sierro, J. Magn. Magn. Mater. **47 & 48**, 526 (1985)
⁹ D. Jaccard et al., J. Magn. Magn. Mater. **47 & 48**, 23 (1985)
¹⁰ D. Jaccard and J. Flouquet, Helv. Phys. Acta. **60**, 108 (1987)
¹¹ D. Jaccard et al., J. Magn. Magn. Mater. **63 & 64**, 572 (1987)
¹² Y. Onuki and T. Komatsubara, J. Magn. Magn. Mater. **63 & 64**, 281 (1987)
¹³ J. Sakurai et al., J. Magn. Magn. Mater. **63 - 64**, 578 (1987)
¹⁴ A. Amato, Thesis, Geneva, 1988
¹⁵ A. Amato et al., J. Magn. Magn. Mater. **76 & 77**, 263 (1988)
¹⁶ C. Fierz et al., J. Appl. Phys. **63**, 3899 (1988),
¹⁷ U. Gottwick et al, J. Magn. Magn. Mater. **63 - 64**, 342 (1987)
¹⁸ J. Sakurai et al, J. Magn. Magn. Mater. **76 - 77**, 287 (1988)
¹⁹ E. V. Sampathkumaran et al., Solid State Commun. **71**, 71 (1989)
²⁰ M.R. Lees, B. R. Coles, E. Bauer and N. Pillmayr, J. Phys.: Condens. Matter, **2**, 6403 (1990);
²¹ R. Casanova et al., J. Magn. Magn. Mater. **90 - 91**, 587 (1990),
²² D. Jaccard, et al. J. Low Temp. Phys. **80**, 285 (1990),
²³ E. Bauer, Adv. Phys. **40**, 417 (1991);
²⁴ R. Cîbin, D. Jaccard and J. Sierro, J. Magn. Magn. Mater. **108**, 107 (1992)
²⁵ D. Jaccard, K. Behnia and J. Sierro, Physics Lett. A **163**, 475 (1992),
²⁶ Y. Bando et al., Physica B **186-188**, 525 (1993)
²⁷ J. Sakurai et al, J. Magn. Magn. Mater. **140 - 144**, 1223 (1995),
²⁸ P. Link, D. Jaccard and P. Lejay, Physica B **225**, 207 (1996),
²⁹ M. Očko, B. Bushinger, C. Geibel and F. Steglich, Physica B **259-261**, 87 (1999),
³⁰ D. Huo, K. Mori, T. Kuwai, S. Fukuda, Y. Isikawa, J. Sakurai, Physica B **281 & 282**, 101 (2000),
³¹ J. Sakurai, D. Huo, D. Kato, T. Kuwai, Y. Isikawa, K. Mori, Physica B **281 & 282**, 98 (2000)
³² M. Očko, D. Drobac, C. Geibel and F. Steglich, Phys. Rev. B **64**, 1151xx (2001).
³³ M. Očko, C. Geibel and F. Steglich, Phys. Rev. B **64**, 1251xx (2001).
³⁴ G. Mahan, B. Sales, and J. Sharp, Physics Today, 42 (1997)
³⁵ I. Peschel and P. Fulde, Z. Phys. **238**, 99 (1970)
³⁶ A.K. Bhattacharjee and B. Coqblin, Phys. Rev. B **13**, 3441 (1976)
³⁷ S. Maekawa et al, J. Phys. Soc. Japan **55** 3194 (1986)
³⁸ N. E. Bickers, D. L. Cox & J. W. Wilkins, Phys. Rev B **36**, 2036 (1987)
³⁹ K. Fischer, Z. Phys. B **76**, 315 (1989)
⁴⁰ R. Monnier et al, Phys. Rev. B **41**, 573 (1990)
⁴¹ S. M. M. Evans, A.K. Bhattacharjee and B. Coqblin, Phys. Rev. B **45**, 7244 (1992)
⁴² V. Zlatić, T. A. Costi, A.C. Hewson and B.R. Coles, Phys. Rev. B **48**, 16523 (1993);
⁴³ T. A. Costi, A. Hewson, and V. Zlatić, J. Phys.: Cond. Matt. **6**, 2519 (1994)
⁴⁴ V. Zlatić and B. Horvatić J. Phys. f **12**, 3075 (1982)
⁴⁵ V. Zlatić and N. Rivier, J. Phys. f **4**, 732 (1974)
⁴⁶ G. Mahan, Solid State Physics **51**, p.82, H. Ehrenreich (ed.), Academic Press 1997
⁴⁷ A. Aviani, M. Miljak, V. Zlatić, D. Schotte, C. Geibel and F. Steglich, Phys. Rev. B **64**, (2001).
⁴⁸ B. Coqblin and J. R. Schrieffer, Phys. Rev. **185**, 847 (1969)
⁴⁹ B. Cornut and B. Coqblin, Phys. Rev. B **5**, 4541 (1972)
⁵⁰ P. W. Anderson, J. Phys. C **3**, 2346 (1970)
⁵¹ Ph. Nozières and A. Blandin, J. Phys. (Paris) **41**, 193 (1980)
⁵² K. Yamada, K. Yosida and K. Hanzawa, Prog. Theor. Phys. **71**, 450 (1984); Prog. Theor. Phys. (Suppl.) **108**, 141 (1992)
⁵³ K. Hanzawa, K. Yamada and K. Yosida, J. Mag. Mag. Matt. **47 & 48**, 357 (1985)
⁵⁴ A. C. Hewson, *The Kondo Problem to Heavy Fermions*, Cambridge University Press (1993)
⁵⁵ H. Schweitzer and G. Czycholl, Phys. Rev. Letters **67**, 3724 (1991)
⁵⁶ Handbook of Mathematical Functions, M. Abramowitz and I. A. Stegun (ed.), Dover (New York, 1965)
⁵⁷ The total potential scattering, $\tilde{V} = V_0 - J_0 < n >$, is scaling invariant, because the scaling equations involve only the traceless part of the Hamiltonian⁵¹.
⁵⁸ W. Metzner, D. Vollhardt, Phys. Rev. Letters **62**, 324 (1989)
⁵⁹ A. Martín-Rodero, E. Louis, F. Flores, and C. Tejedor, Phys. Rev. B **33**, 1814 (1986);